Draft version May 8, 2013
Preprint typeset using LaTeX style emulateapj v. 5/2/11

arXiv:1305.1325v1 [astro-ph.CO] 6 May 2013

POPULATION III STARS AND REMNANTS IN HIGH REDSHIFT GALAXIES

Hao Xu[1], John H. Wise[2], and Michael L. Norman[1]

Draft version May 8, 2013

ABSTRACT

Recent simulations of Population III star formation have suggested that some fraction form in binary systems, in addition to having a characteristic mass of tens of solar masses. The deaths of metal-free stars result in the initial chemical enrichment of the universe and the production of the first stellar-mass black holes. Here we present a cosmological adaptive mesh refinement simulation of an overdense region that forms a few 10^9 $M_\odot$ dark matter halos and over 13,000 Population III stars by redshift 15. We find that most halos do not form Population III stars until they reach $M_{\rm vir} \sim 10^7$ $M_\odot$ because this biased region is quickly enriched from both Population III and galaxies, which also produce high levels of ultraviolet radiation that suppress H_2 formation. Nevertheless, Population III stars continue to form, albeit in more massive halos, at a rate of $\sim 10^{-4} M_\odot\,{\rm yr}^{-1}\,{\rm Mpc}^{-3}$ at redshift 15. The most massive starless halo has a mass of 7×10^7 $M_\odot$, which could host massive black hole formation through the direct gaseous collapse scenario. We show that the multiplicity of the Population III remnants grows with halo mass above 10^8 $M_\odot$, culminating in 50 remnants located in 10^9 $M_\odot$ halos on average. This has implications that high mass X-ray binaries and intermediate mass black holes that originate from metal-free stars may be abundant in high-redshift galaxies.

Subject headings: cosmology – methods: numerical – hydrodynamics – radiative transfer – star formation

1. INTRODUCTION

The first generation stars (Population III) form from metal-free gas in dark matter halos with $M \sim 10^6$ $M_\odot$ and have a large characteristic mass (e.g. Abel et al. 2002; Bromm et al. 2002; O'Shea & Norman 2007; Turk et al. 2009; Greif et al. 2012). Due to their high mass, they have short lifetimes (Schaerer 2002) and may go supernova, and enrich their surrounding intergalactic medium (IGM). For these metal-free stars, Type II supernovae (SNe) happen for an initial mass between 10 and 40 $M_\odot$, and much more energetic pair-instability SNe (PISNe) might occur in stars between 140 and 260 $M_\odot$ Heger et al. (2003). Once the metallicity passes some critical metallicity, $\sim 10^{-6}$ $Z_\odot$ if dust cooling is efficient (Omukai et al. 2005; Schneider et al. 2006; Clark et al. 2008) or $\sim 10^{-3.5}$ $Z_\odot$ otherwise (Bromm et al. 2001; Smith et al. 2009), the gas can cool rapidly and lower its Jeans mass. These metal-enriched (Population II) stars have a lower characteristic mass scale and most likely have an initial mass function (IMF) that resembles the present-day one. However at high redshift, heating from the cosmic microwave background (CMB) may limit the radiative cooling, and thus increasing the Jeans mass, resulting in an IMF that also favors massive star formation (Larson 2005; Smith et al. 2009).

The transition from Pop III to Pop II star formation is solely dependent on the metal enrichment from the Pop III SN remnants in the future star forming halos. Metal enrichment involves complex interactions between SNe blastwaves, the intergalactic medium (IGM), halo mergers, and cosmological accretion. This topic has been extensively studied with semi-analytic models (Scannapieco et al. 2003; Yoshida et al. 2004; Tumlinson 2006; Salvadori et al. 2007; Komiya et al. 2010), post-processing of numerical simulations (Karlsson et al. 2008; Trenti et al. 2009), and direct numerical simulations (Tornatore et al. 2007; Ricotti et al. 2008; Maio et al. 2010; Wise et al. 2012b; Muratov et al. 2012). For example, Trenti et al. (2009) suggested that Pop III stars may still form at the late epoch of $z = 6$ in the under dense regions of the universe by post-processing of cosmological simulations with blast wave models. Muratov et al. (2012) also showed that Pop III stars continue to form until $z = 6$ using direct cosmological simulations.

In addition to the metal enrichment from Pop III stars, heating and ionizing effects from their radiation are crucial to modeling early structure formation of the Universe. (Haiman et al. 2000). Lyman-Werner photons from Pop III stars photodissociate H_2 by the Solomon process and suppress the formation of Pop III stars in low-mass halos. The higher energy UV radiation from Pop III stars then affects the subsequent structure formation through heating and ionizing the surrounding IGM (Machacek et al. 2001; Yoshida et al. 2003; Wise & Abel 2007; O'Shea & Norman 2008). Pop III more massive than 260 $M_\odot$ or less massive than 140 $M_\odot$ may direct collapse to form black holes Heger et al. (BHs; 2003). Accretion onto these massive Pop III BHs is a feasible way to form $z > 7$ quasars (Johnson et al. 2012) and is also an important source of X-ray radiation in high redshifts. X-rays from the accretion onto Pop III BHs (Alvarez et al. 2009) or from Pop III binaries (Turk et al. 2009; Stacy et al. 2010; Stacy & Bromm 2012) may preheat and pre-ionize a large volume of the IGM (Ricotti & Ostriker 2004; Mesinger et al. 2013).

[1] Center for Astrophysics and Space Sciences, University of California, San Diego, 9500 Gilman Drive, La Jolla, CA 92093; hxu@ucsd.edu, mlnorman@ucsd.edu
[2] Center for Relativistic Astrophysics, School of Physics, Georgia Institute of Technology, 837 State Street, Atlanta, GA 30332; jwise@gatech.edu

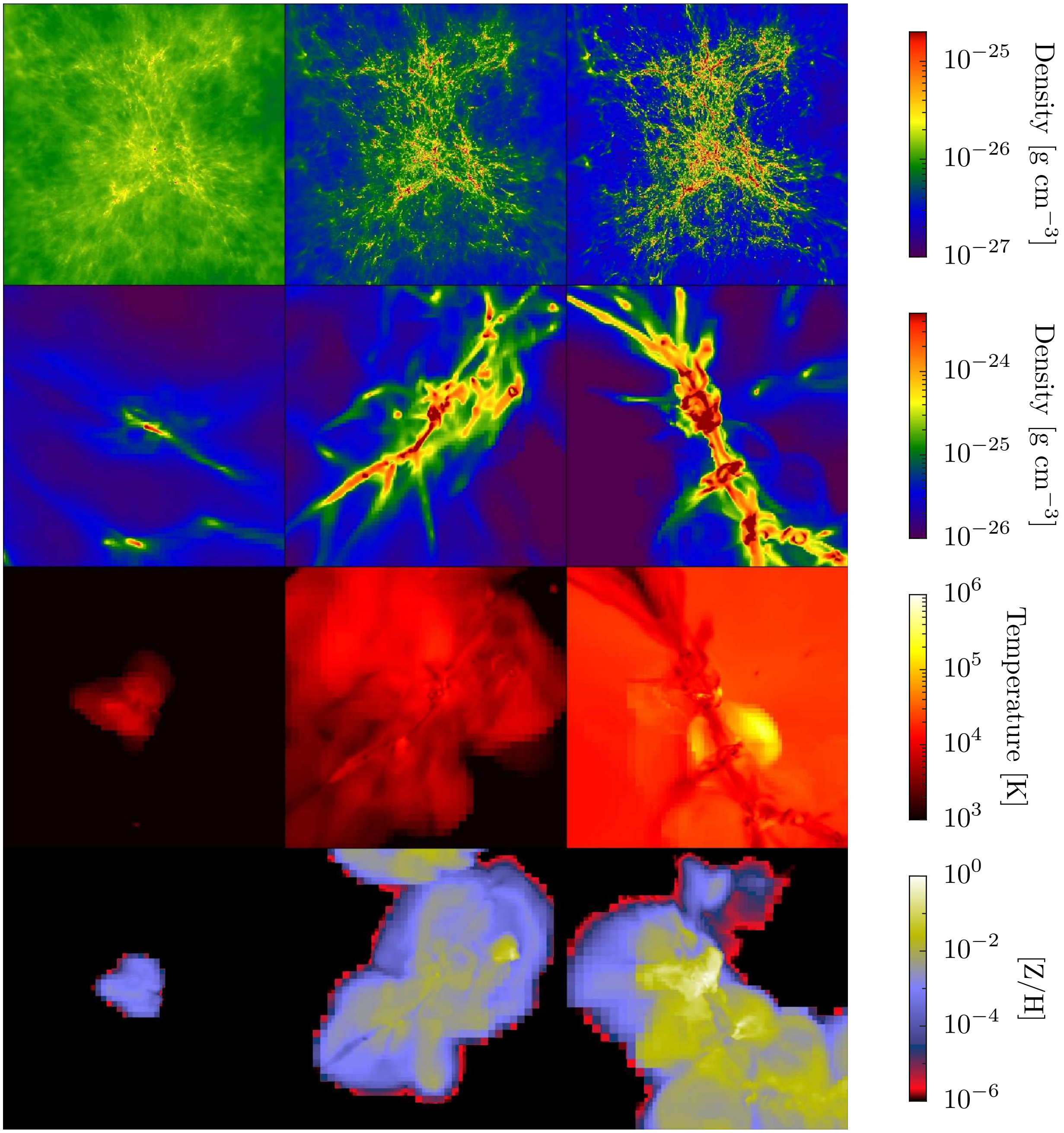

Figure 1. Snapshots of the refined regions and the most massive halos at redshifts 25 (left), 17.91 (middle) and 15 (right). The images are the density-weighted projections of baryon density in cubic volumes 6.6 comoving Mpc on a side (first row), enclosing the refined regions, the density-weighted projections of baryon density (second row), temperature (third row) and metallicity (fourth row) in cubic volumes 10.0 proper kpc on a side, enclosing the most massive halos.

The impact of Pop III feedback on cosmic evolution is dependent on the properties of their host halos, especially their masses (Whalen et al. 2008; Muratov et al. 2012). The sizes of the host halos determine the distance the metal from Pop III SNe reach with their blast waves, and the escape faction of their UV radiation. This makes a detailed study of the Pop III star and remnant distribution over a wide range of high redshift galaxies necessary.

It is impossible to observe of Pop III stars during their lifetime at high redshift, but they might still possibly be detected directly by looking for their PISN explosions before their death. This idea has been studied and shown to be promising for both LSST (Trenti et al. 2009) and JWST (Hummel et al. 2012; Whalen et al. 2013). Understanding the population and distribution of Pop III stars and remnants in high redshift galaxies is helpful for preparing the observation of these events.

In this paper, we focus on the the formation of Pop III stars and the population and multiplicity of Pop III stars and remnants in high redshift galaxies. We have performed a simulation of a survey volume of over 100 comoving Mpc^3 that includes a full primordial chemistry network, radiative cooling from metal species, both Pop

II and Pop III star formation and their radiative, thermal, mechanical and chemical feedback. The simulation runs on such a large volume from cosmological initial conditions, so that we can follow the formation and fate of Pop III stars in a statistically significant number of halos with a wide range of masses from a few million solar mass to one billion solar mass. We first describe our simulation model in Section 2. Then in Section 3, we present our results of the Pop III stars and remnants distribution over early galaxies. We discuss the findings and possible bias in our simulation in Section 4.

2. SIMULATION SETUP

We perform the simulation using the adaptive mesh refinement (AMR) cosmological hydrodynamics code Enzo (O'Shea et al. 2004). Adaptive ray tracing (Wise & Abel 2011) is used for the radiation transfer of ionizing radiation, which is coupled to the hydrodynamics and chemistry in Enzo. The chemistry, cooling, and star formation and feedback models used in this simulation are the same as in Wise et al. (2012b).

We generate the initial conditions for the simulation using Music (Hahn & Abel 2011) at $z = 99$ and use the cosmological parameters from the 7-year WMAP ΛCDM+SZ+LENS best fit (Komatsu et al. 2011): Ω_M=0.266, Ω_Λ = 0.734, Ω_b=0.0449, h=0.71, σ_8=0.81, and n=0.963. We use a comoving simulation box of (40 Mpc)^3 that has a 512^3 root grid resolution and three levels of static nested grids. We first run a 512^3 N-body only simulation to $z = 6$. Then we select the Lagrangian volume around two $\sim 3\times10^{10}$M$_\odot$ halos at $z = 6$, and re-initialize the simulation with 3 more nested grids to have an effective resolution of 4096^3 and an effective dark matter mass resolution of 2.9×10^4M$_\odot$ inside the highest nested grid of 300 comoving Mpc^3. During the course of the simulation, we allow a maximum refinement level $l = 12$, resulting in a maximal resolution of 19 comoving kpc. The refinement criteria employed are also the same as in Wise et al. (2012b), but the refinements higher than the static nested grids are only allowed in the region that contains only high resolution particle, that is ~ 150 comoving Mpc^3 at $z = 15$. At this time, the simulation has a large number (∼1000) of halos with M $> 10^8$ M$_\odot$, where new formation of Pop III stars declines rapidly, for statistical analysis. We use results at this redshift for our current study. The simulation has 1.3 billion computational cells and required more than 10 million CPU hours, and there are three $> 10^9$ M$_\odot$ halos in the refined regions at this time. We will continue this simulation to lower redshift for the study of the Pop II stars and high redshift galaxies.

Both Pop II and Pop III stars form in the simulation, and we distinguish them by the total metallicity of the densest star forming cell. Pop III stars are formed if [Z/H] > -4, and Pop II stars are formed otherwise. We use the same star formation models and most of the parameters in Wise et al. (2012b), as well as feedback models. The only difference between the two simulations is that we use a characteristic mass of 40 M$_\odot$ for the Pop III IMF, which is more in line with the latest results of Pop III formation simulations (e.g. Turk et al. 2009; Greif et al. 2012), instead of 100 M$_\odot$. Please see Section 2.2 and Section 2.3 of Wise et al. (2012b), for the details of the star formation and stellar feedback used in the simulation, respectively.

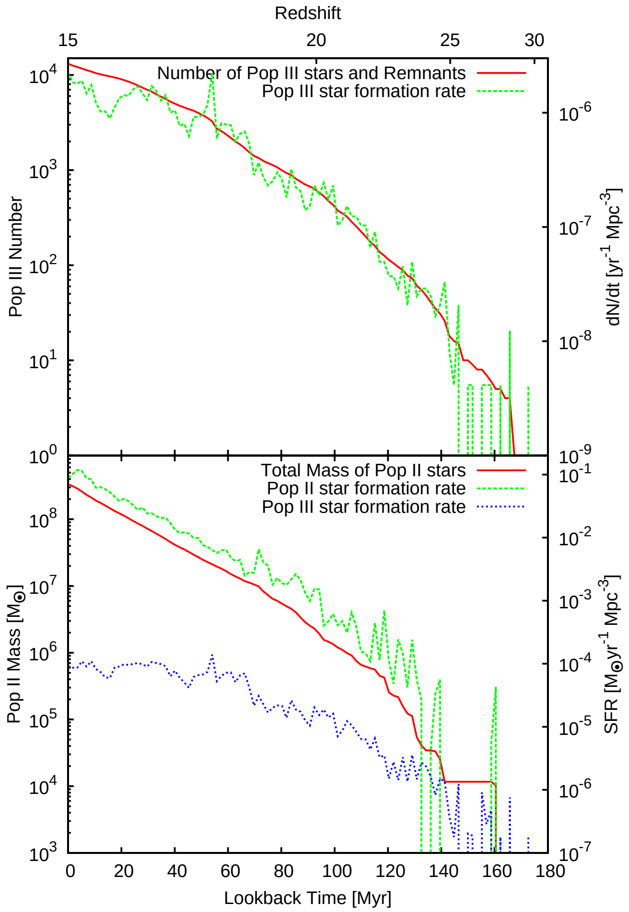

Figure 2. Top panel: Evolution of the cumulative number of Population III stars and remnants and the averaged Pop III star number formation rate inside the survey volume. Bottom panel: Evolution of the total Pop II star mass, and the Pop II and Pop III star formation rate by mass. The mass formation rate of Pop III stars depends on the choice of M$_{char}$.

We show the evolution of the high-resolution region in Figure 1 at three redshifts, 25, 17.91, and 15. Here we show the large scale structure in the inner 6.6 comoving Mpc in the top row, and in the remaining rows, we focus on the most massive halo at each redshift by showing their density-weighted projections of gas density, temperature, and metallicity.

3. RESULTS

We illustrate the evolution of the number of Pop III stars and remnants, as well as their formation rate from the birth of the first Pop III star to $z = 15$ in the top panel of Figure 2. Massive Pop III stars have very short lifetimes (Schaerer 2002) and end their life by either directly collapsing to black holes or exploding as supernovae (Heger et al. 2003), depending on their initial masses. More specifically, they die as Type II SNe if 11 $\leq$ M$_\star$ / M$_\odot$ $\leq$ 40 and as PISNe if 140 $\leq$ M$_\star$ / M$_\odot$ $\leq$ 260, where M$_\star$ is the initial stellar mass, or become black holes if their masses are not in these mass ranges. Throughout the paper, we use "Pop III remnants" to refer to all remains of dead Pop III stars, regardless whether they become black holes or supernova remnants, and we use "Pop III" to refer to *both* living stars and dead remnants.

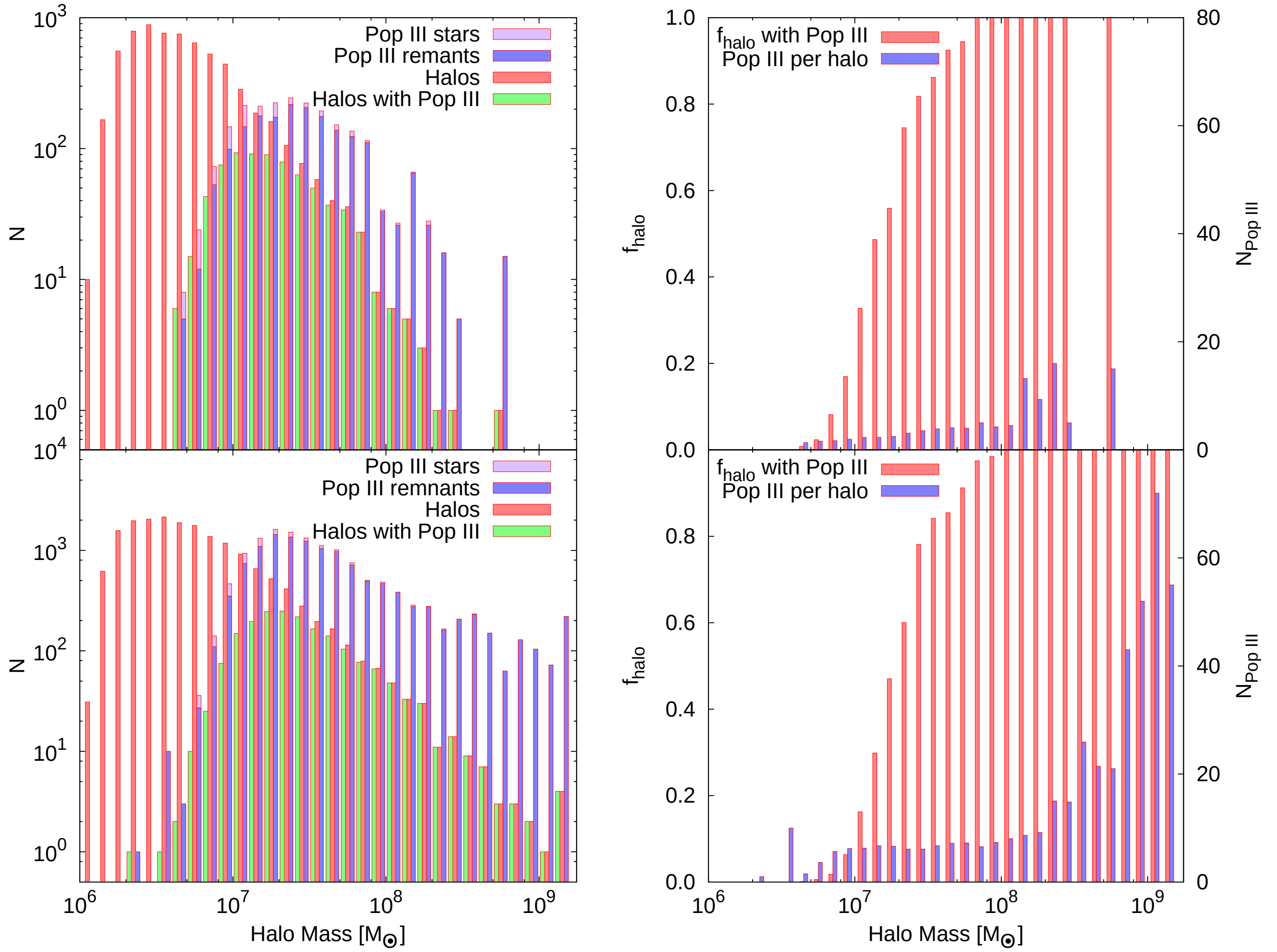

Figure 3. Left panel: Number of Pop III, total halos and halos with Pop III as functions of halo mass at redshifts 17.91 (Top) and 15 (Bottom). The number of living Pop III stars are stacked over the Pop III remnants showing in the same bin. Right panel: Fraction of halos hosting Pop III and average number of Pop III per halo at redshift 17.91 (Top) and 15 (Bottom).

In the case that remnants have negligible masses after SN events, their star masses are replaced with a very small mass proportional to their initial masses and the star particles are kept in the simulation to follow their remnant kinematic distribution. The first Pop III star forms at redshift $z \sim 29.7$. Rates of Pop III star formation steadily increase from $\sim 10^{-8}$ to above 10^{-6} stars per year per comoving Mpc^3. The Pop III star formation rate shows some signs of saturation at $z \sim 15$ in this overdense region of the universe. At $z = 15$, the entire survey volume of 138 comoving Mpc^3 contains 13,123 Pop III stars and remnants and 7,677 halos more massive than 5×10^6 M$_\odot$. The number densities of Pop III and halos that host Pop III are 95 and 55 per comoving Mpc^3, respectively.

The total mass of Pop II stars and the SFR of Pop II and Pop III are shown in the bottom panel of Figure 2. There is $\sim 3 \times 10^8$ M$_\odot$ mass in Pop II stars at $z = 15$. The star formation histories for both Pop II and Pop III stars are similar to those in Wise et al. (2012b), but shifted to higher redshifts. We will study the details of Pop II star formation in this simulation in a forthcoming paper.

We show the number of Pop III, all halos, and star-hosting halos as function of halo mass inside the survey volume at $z = 17.91$ and $z = 15$ in the left panels in Figure 3, while the numbers of living Pop III stars are stacked over remnants in the same bin. In the right panels in Figure 3, shown are the fraction of halos hosting Pop III and the average Pop III per halo (over halos having Pop III) as functions of halo mass.

As our survey volume is chosen over a high density region, the halo number density is higher than the Universe mean. The halo mass functions from our simulation are well fit with the fitting function of Warren et al. (2006) boosted by a factor of five for halos heavier than 5×10^6 M$_\odot$ in both redshifts. The number of halos drops for halos $< 5 \times 10^6$ M$_\odot$, due to the lack of dark matter mass resolution. At $z = 15$, our simulation has a factor of a few more halos than the prediction from the fitting function for halos more massive than 1×10^8 $M_\odot$, showing that the baryon becomes important in massive halos. There are 3 halos with masses over 10^9 M$_\odot$ at $z = 15$, while the first one appears at redshift $z \sim 15.8$.

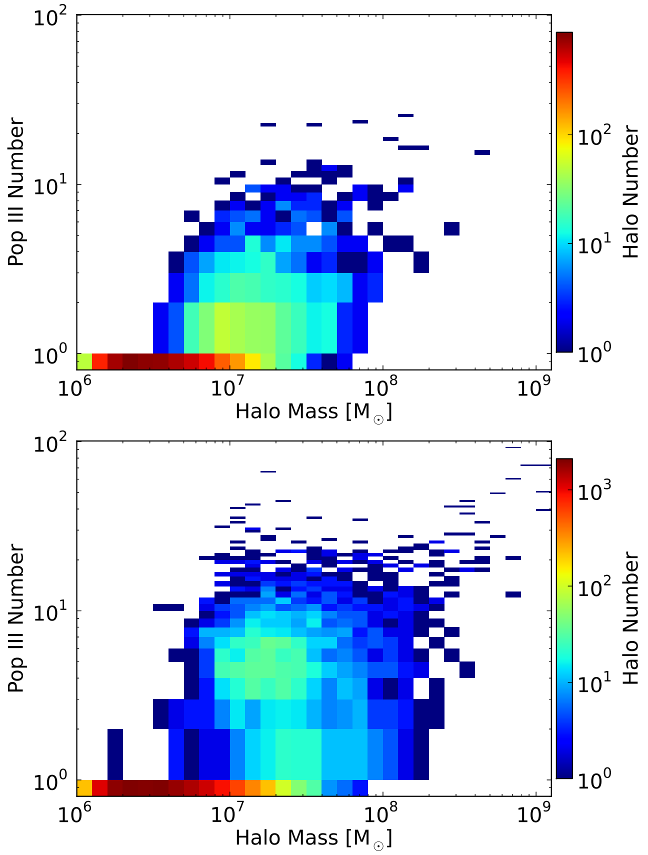

Figure 4. Phase plots of halo number indicating the distribution of Pop III stars and remnants over halos as a function of PopIII number and their host halo mass at redshifts 17.91 (Top) and 15 (Bottom).

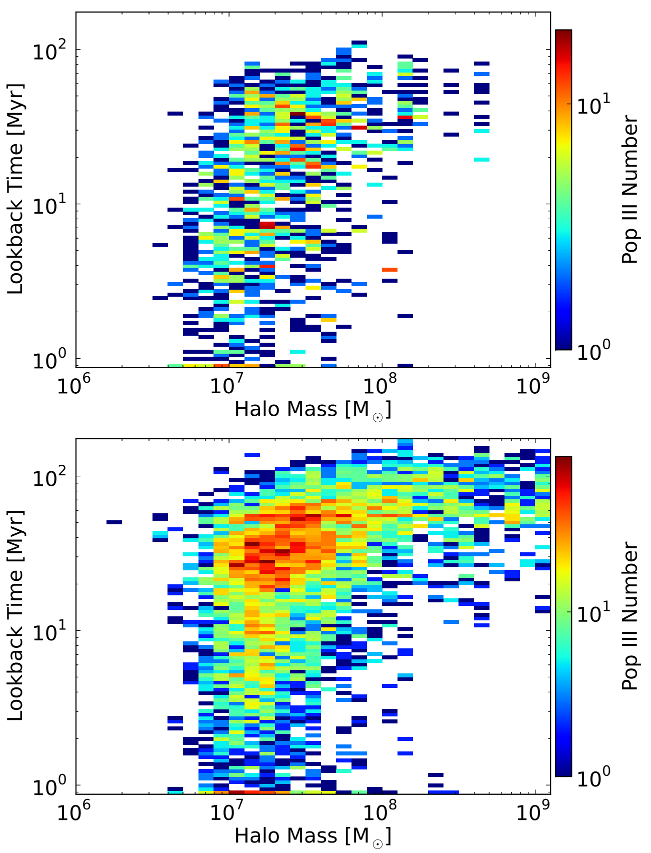

Figure 5. Phase plots of Pop III number indicating the relation between Pop III formation and host halo mass as a function of PopIII star formation time and their host halo mass at redshifts 17.91 (Top) and 15 (Bottom).

The Pop III distribution over halo mass shows little evolution, except that there are more Pop III appearing in high mass halos as those halos building up with time. The number of Pop III peaks at $\sim 3 \times 10^7$ M$_\odot$. The fraction of halos hosting Pop III also has little change between redshifts 17.91 and 15 because the chances to host Pop III are very small for halos less massive than 10^7 M$_\odot$ in this biased region. Then they gradually increases with halo mass and reach 100% for halos $\sim 10^8$ M$_\odot$. In this particular mass range of 10^7-10^8M$_\odot$, halos can cool and collapse regardless of the LW background and form stars (e.g. Wise & Abel 2007; O'Shea & Norman 2008; Shang et al. 2010; Wolcott-Green et al. 2011). The exact timing of Pop III star formation depends on the local strength of the LW intensity, causing the gradual increase in the fraction shown in Figure 3. In addition to H_2 suppression, nearby galaxies and Pop III supernova can chemical enrich halos so that they form metal-enriched stars in their first star formation event without hosting any prior Pop III star formation. Afterwards, as halos grow through hierarchical mergers, the number of Pop III per halos increase with both redshift and halo mass. At z = 15, halos between 10^7 M$_\odot$ and 10^8 M$_\odot$ have an average of 10 Pop III, and the number rises to about 50 for halos $\sim 10^9$ M$_\odot$.

Shown in Figure 4 are the number distribution of halos as a function of halo mass and number of Pop III stars and remnants per halo. The number of PopIII that is hosted by halos inside a mass bin is very scattered, but there is a clear trend that more massive halos host more Pop III stars and remnants. The same trend is shown in the average number of Pop III per halo in Figure 3. At redshift z = 15, the most massive halo without any Pop III stars or remnants is 7.16×10^7 M$_\odot$. On the low mass end, the least massive halo hosting Pop III is only 1.82×10^6 M$_\odot$. But this Pop III star forms at about 50 Myr ago, so this star most likely forms in another more massive halo, then is stripped out with its current host halo from the massive one.

In Figure 5, we show the number distribution of Pop III as function of their host halo mass and their formation time. As old Pop III remnants can be found in halos of all masses, young stars and remnants can only be seen in low mass halos. No Pop III star forms in halos more massive than 3×10^8 M$_\odot$. The gas in massive halos is enriched by their earlier Pop III, so the further formation of stars transitions to Pop II. The least massive halos having newly formed Pop III stars is $\sim 4 \times 10^6$

$M_\odot$, as the Pop III formation in smaller halos is suppressed by the LW background. But our results for Pop III formation in low mass halos might be biased. Due to the relatively low dark matter (2.9×10^4 $M_\odot$), we may miss the formation of $M \lesssim 10^6 M_\odot$ halos in our simulation. We discuss this issue in the next section and show that very little Pop III star formation is missed by the current simulation due to resolution effects.

4. DISCUSSIONS AND CONCLUSIONS

We present results of a cosmological simulation representing a high density region of an unprecedented large volume in the early universe to study the Pop III star and remnant population and multiplicity within high redshift galaxies. The highly resolved simulation volume covers thousand of halos and Pop III stars and remnants, allowing us to make a detailed study of the Pop III star formation history and the Pop III stars and remnants distribution over a wide range of halo masses. We observe a continuous Pop III star formation from z $\sim$ 30 to z $\sim$ 15, when the calculation was paused for analysis. We expect Pop III star formation to continue to lower redshifts, but this needs to be verified by running the simulation further. We find that the number of the Pop III stars and remnants peaks in halos with masses of a few $\times$ 10^7 $M_\odot$ during this time, while the ratio to host Pop III and multiplicity of Pop III increase with the halo mass. The Pop III inside a massive halos are likely coming from mergers of small ones, instead of forming in the big ones. New Pop III stars only form in halos between 4×10^6 to 3×10^8 $M_\odot$, while the formation rate peaks at $\sim 10^7$ $M_\odot$. So even though there are tens of Pop III remnants in a halo of 10^9 $M_\odot$, little to no feedback might be expected coming from their still living Pop III stars.

The dark matter mass resolution in this simulation is not high enough to capture all of the Pop III star forming halos smaller that a few $\times 10^6$ $M_\odot$, so we could be underestimating the number of Pop III in our simulation.

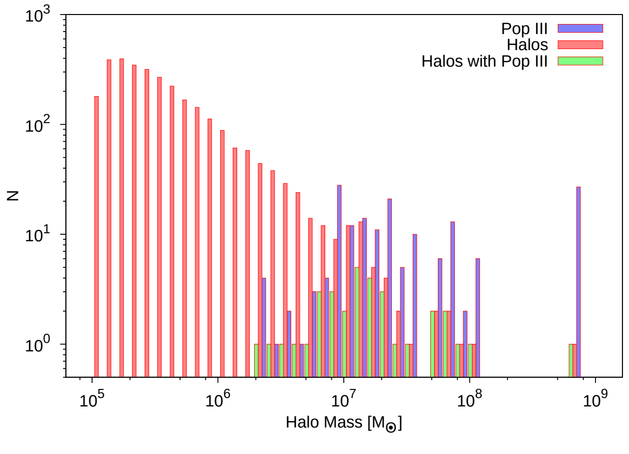

Figure 6. Number of Pop III stars and remnants, all halos, and halos with Pop III as functions of halo mass of the 1 comoving Mpc^3 simulation in Wise et al. (2012b) at redshift 7.28. With a dark matter mass resolution that is finer by a factor of 16, the halo population extends from 10^6 $M_\odot$ to 2×10^5 $M_\odot$. However, there are no Pop III present in those small halos, which are suppressed by a LW background. Indeed, the distribution of Pop III is similar to our current results shown in Figure 3, though two survey volumes are in very different density fluctuations.

To investigate this, we use the simulation in Wise et al. (2012a) to estimate the missing Pop III stars and remnants in low mass halos. We show the histogram of halo mass in that 1 comoving Mpc^3 box simulation at $z = 7.28$ in Figure 6. Due to the much higher dark matter mass resolution, there are many more halos at a few 10^6 $M_\odot$, extending to $\sim 2 \times 10^5$ $M_\odot$. Since the simulation box is small, the halo mass function is not well fit by the Warren et al. (2006) function by having too many low mass halos and too few high mass halos, but still has the number of halos $\sim 10^6$ $M_\odot$ close to cosmic mean. Though there are much less halos and Pop III in this smaller simulated volume, it has a similar distribution of Pop III stars and remnants as in our current simulation. Halos with $M_{\rm halo} \lesssim 2 \times 10^6 M_\odot$ do not host any Pop III stars or remnants in this small box simulation. Pop III star formation in these low-mass halos is suppressed when the H_2 is dissociated by LW radiation from nearby stellar sources and the background (Machacek et al. 2001; Wise & Abel 2007; O'Shea & Norman 2008). The first star forms at $z \sim 20$, when the LW background is already at an intensity of $\sim 10^{-23}$ erg s^{-1} cm^{-2} Hz^{-1} sr^{-1}, and suppresses any H_2 formation and thus Pop III star formation in

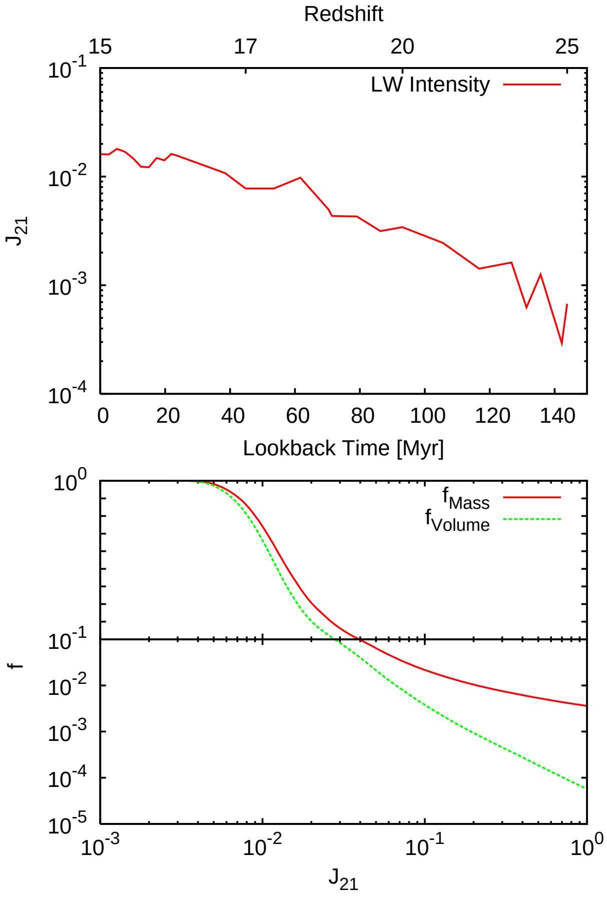

Figure 7. Top panel: Evolution of the volume averaged Lyman-Werner radiation intensity from stars in the simulation. Bottom panel: Complementary cumulative distributions of the LW intensity at $z = 15$. J_{21} is the LW intensity in the unit of 10^{-21} erg s^{-1} cm^{-2} Hz^{-1} sr^{-1}. The averaged LW intensity gradually increases to and maintains above 10^{-23} erg s^{-1} cm^{-2} Hz^{-1} sr^{-1} for the last 40 Myr. This LW radiation is not enough to significantly slow down the Pop III formation.

halos below a mass of $10^6 \mathrm{M}_\odot$. At later times, we also confirm that the minimum star-forming halo mass with this LW background in Wise et al. (2012a) at any time is $\gtrsim 10^6 \mathrm{M}_\odot$. Thus, we conclude that the Pop III formation rate is small in halos below this mass scale and that we do not miss a significant fraction of Pop III star formation in our simulation because of mass resolution.

In this large volume simulation, only the LW flux from point sources is included, while the LW background is ignored. We show the evolution of averaged LW intensity and the fraction distribution of LW intensity at $z = 15$ over the refined volume in Figure 7. The averaged LW radiation intensity builds up gradually and reaches 10^{-23} erg s^{-1} cm^{-2} Hz^{-1} sr^{-1}at redshift $z \sim 17$, and maintains at this level for more than 40 Myr. At $z = 15$, the LW intensity in $\sim 70\%$ of the volume is higher than 10^{-23} erg s^{-1} cm^{-2} Hz^{-1} sr^{-1}, while only less than 0.01% of the volume (0.014 comoving $(\mathrm{Mpc})^3$) is filled with LW radiation stronger than 10^{-21} erg s^{-1} cm^{-2} Hz^{-1} sr^{-1}. This LW intensity, locally produced even in a rare high density region, is still weaker than the expected LW background (Wise & Abel 2005; Wise et al. 2012a), and, though it suppresses Pop III formation in 10^6 $M_\odot$ halos, is not strong enough to have significant impact on the Pop III formation in larger halos.

An important difference between the simulation in this paper and that of Wise et al. (2012a) is that the characteristic mass of Pop III stars here is much lower at $\mathrm{M}_{char} = 40$ $\mathrm{M}_\odot$, instead of $\mathrm{M}_{char} = 100$ $\mathrm{M}_\odot$. The new choice of characteristic mass results that much fewer Pop III stars have initial mass between 140 and 260 $\mathrm{M}_\odot$, and end their life by PISN. This then significantly reduces the metal generated by Pop III stars. For example, a 40 $\mathrm{M}_\odot$ hypernova produces only 8.6 $\mathrm{M}_\odot$ metals (Nomoto et al. 2006), comparing to 85 $\mathrm{M}_\odot$ of metals generated by 180 $\mathrm{M}_\odot$ PISN (Heger & Woosley 2002). It is likely due to the lower level of metal generation, that Pop III stars continue to form in the larger halos ($> 10^8$ $\mathrm{M}_\odot$) in current simulation. On the contrary, there is no Pop III formed in halos more massive than 5×10^7 $\mathrm{M}_\odot$ in Wise et al. (2012b).

Because our simulation covers a rare high density region, our results are not representative of the cosmic mean. We fit the halo mass function with the fitting function of Warren et al. (2006). It shows that the halo number density at $z = 15$ is about five times that of the cosmic mean at the same redshift or about the cosmic mean at $z = 10$, while the halo number density at $z = 17.91$ is about the cosmic mean at $z = 14$. The density fluctuations may have effects on local Pop III formation by changing the LW background and metallicity level of the IGM. As discussed before, the strength of LW background during these redshifts might not change the Pop III formation significantly. In addition, because the mean distance between Pop III and halos is still much larger than the direct metal impact distance of a PISN of 5 kpc (Wise et al. 2012b), the metal enrichment by Pop III feedback crossing halos is still weak, except in halo clusters. In the case, the Pop III formation mostly depends on single halo properties, while the multiplicity of Pop III over halos is determined by the clustering of halos. Our results of Pop III distribution and multiplicity over halos should not change significantly in regions of different density fluctuations. The population of Pop III is proportional to the halo density, so the number density from this simulation at $z = 15$ should be about 5 times that of the cosmic mean or close to the cosmic mean at z $\sim$ 10.

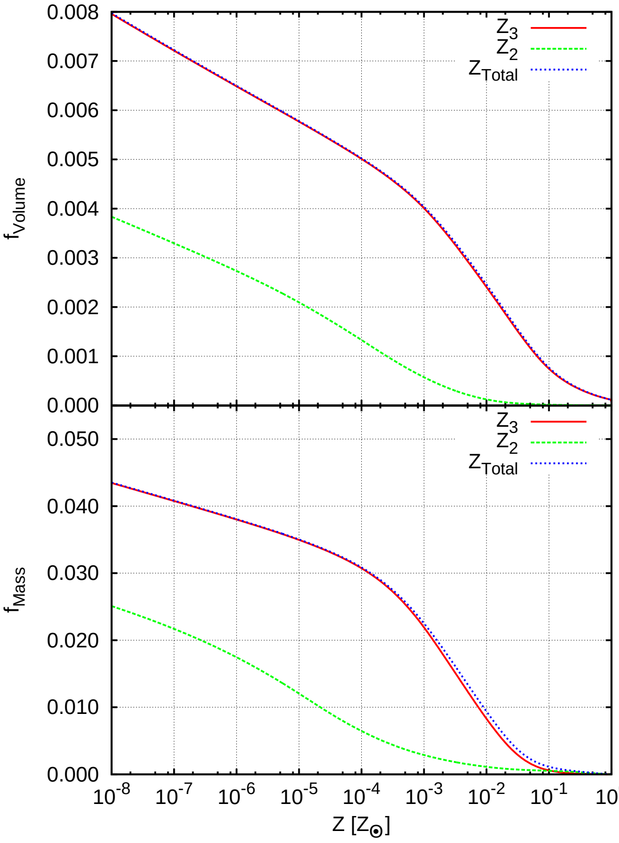

Figure 8. Complementary cumulative distributions of the metallicity by volume (Top) and by mass (Bottom) inside the refined region at $z = 15$. The solid, dashed, dotted lines show the metal from Pop III stars, Pop II stars, and the total metal, respectively. The total metallicity distributions are still determined by the feedback from Pop III stars at this epoch.

One important question about Pop III stars is when and in what environments their formation completely ends. Unfortunately, our simulation does not show the cessation, or even the saturation of Pop III formation yet, though the increase of star formation rate slows down in the last tens of million years. The Pop III star and remnant number density is still low (lower than that of Wise et al. (2012b) 1 Mpc^3 simulation), and there still is a significant fraction of halos between 10^7 and 10^8 $\mathrm{M}_\odot$ that have no Pop III stars and are in a favorable LW radiation field. To show the sufficiency of metal poor gas inside the survey volume to continue form Pop III stars, we plot the volume and mass complementary cumulative distributions of the metallicity at $z = 15$ in Figure 8. There are only about 0.65% of volume and 3.8% of the mass enriched above 10^{-6} $\mathrm{Z}_\odot$. For comparison, the Wise et al. (2012b) 1 Mpc^3 simulation has 0.32% of the volume and 2.6% of the mass at $z = 10$, and 0.89% of the volume and 7.6% of the mass at $z = 7.28$, respectively, above 10^{-6} $Z_{\odot}$. So it is reasonable to expect Pop III stars will continue to form inside our survey volume, but at a constant rate, since Wise et al. (2012b) shows that the Pop III formation rate is constant from $z = 12$ to 7. We are continuing the present simulation to lower redshifts to confirm or deny this expectation.

This research was supported by National Science Foundation (NSF) grant AST-1109243 to MLN. JHW acknowledges support from NSF grant AST-1211626. The simulation was performed on the Kraken supercomputer operated for the Extreme Science and Engineering Discovery Environment (XSEDE) by the National Institute for Computational Science, ORNL with XRAC allocation MCA-TG98020N.

REFERENCES

Abel, T., Bryan, G. L., & Norman, M. L. 2002, Science, 295, 93
Alvarez, M. A., Wise, J. H., & Abel, T. 2009, ApJ, 701, L133
Bromm, V., Coppi, P. S., & Larson, R. B. 2002, ApJ, 564, 23
Bromm, V., Ferrara, A., Coppi, P. S., & Larson, R. B. 2001, MNRAS, 328, 969
Clark, P. C., Glover, S. C. O., & Klessen, R. S. 2008, ApJ, 672, 757
Greif, T. H., Bromm, V., Clark, P. C., Glover, S. C. O., Smith, R. J., Klessen, R. S., Yoshida, N., & Springel, V. 2012, MNRAS, 424, 399
Hahn, O., & Abel, T. 2011, MNRAS, 415, 2101
Haiman, Z., Abel, T., & Rees, M. J. 2000, ApJ, 534, 11
Heger, A., Fryer, C. L., Woosley, S. E., Langer, N., & Hartmann, D. H. 2003, ApJ, 591, 288
Heger, A., & Woosley, S. E. 2002, ApJ, 567, 532
Hummel, J. A., Pawlik, A. H., Milosavljević, M., & Bromm, V. 2012, ApJ, 755, 72
Johnson, J. L., Whalen, D. J., Li, H., & Holz, D. E. 2012, ArXiv e-prints
Karlsson, T., Johnson, J. L., & Bromm, V. 2008, ApJ, 679, 6
Komatsu, E., Smith, K. M., Dunkley, J., Bennett, C. L., Gold, B., Hinshaw, G., Jarosik, N., Larson, D., Nolta, M. R., Page, L., Spergel, D. N., Halpern, M., Hill, R. S., Kogut, A., Limon, M., Meyer, S. S., Odegard, N., Tucker, G. S., Weiland, J. L., Wollack, E., & Wright, E. L. 2011, ApJS, 192, 18
Komiya, Y., Habe, A., Suda, T., & Fujimoto, M. Y. 2010, ApJ, 717, 542
Larson, R. B. 2005, MNRAS, 359, 211
Machacek, M. E., Bryan, G. L., & Abel, T. 2001, ApJ, 548, 509
Maio, U., Ciardi, B., Dolag, K., Tornatore, L., & Khochfar, S. 2010, MNRAS, 407, 1003
Mesinger, A., Ferrara, A., & Spiegel, D. S. 2013, MNRAS
Muratov, A. L., Gnedin, O. Y., Gnedin, N. Y., & Zemp, M. 2012, ArXiv e-prints
Nomoto, K., Tominaga, N., Umeda, H., Kobayashi, C., & Maeda, K. 2006, Nuclear Physics A, 777, 424
Omukai, K., Tsuribe, T., Schneider, R., & Ferrara, A. 2005, ApJ, 626, 627
O'Shea, B. W., Bryan, G., Bordner, J., Norman, M. L., Abel, T., Harkness, R., & Kritsuk, A. 2004, ArXiv Astrophysics e-prints (astro-ph/0403044)
O'Shea, B. W., & Norman, M. L. 2007, ApJ, 654, 66
—. 2008, ApJ, 673, 14
Ricotti, M., Gnedin, N. Y., & Shull, J. M. 2008, ApJ, 685, 21
Ricotti, M., & Ostriker, J. P. 2004, MNRAS, 352, 547
Salvadori, S., Schneider, R., & Ferrara, A. 2007, MNRAS, 381, 647
Scannapieco, E., Schneider, R., & Ferrara, A. 2003, ApJ, 589, 35
Schaerer, D. 2002, A&A, 382, 28
Schneider, R., Omukai, K., Inoue, A. K., & Ferrara, A. 2006, MNRAS, 369, 1437
Shang, C., Bryan, G. L., & Haiman, Z. 2010, MNRAS, 402, 1249
Smith, B. D., Turk, M. J., Sigurdsson, S., O'Shea, B. W., & Norman, M. L. 2009, ApJ, 691, 441
Stacy, A., & Bromm, V. 2012, ArXiv e-prints
Stacy, A., Greif, T. H., & Bromm, V. 2010, MNRAS, 403, 45
Tornatore, L., Ferrara, A., & Schneider, R. 2007, MNRAS, 382, 945
Trenti, M., Stiavelli, M., & Shull, J. M. 2009, ApJ, 700, 1672
Tumlinson, J. 2006, ApJ, 641, 1
Turk, M. J., Abel, T., & O'Shea, B. 2009, Science, 325, 601
Warren, M. S., Abazajian, K., Holz, D. E., & Teodoro, L. 2006, ApJ, 646, 881
Whalen, D., O'Shea, B. W., Smidt, J., & Norman, M. L. 2008, ApJ, 679, 925
Whalen, D. J., Fryer, C. L., Holz, D. E., Heger, A., Woosley, S. E., Stiavelli, M., Even, W., & Frey, L. H. 2013, ApJ, 762, L6
Wise, J. H., & Abel, T. 2005, ApJ, 629, 615
—. 2007, ApJ, 671, 1559
—. 2011, MNRAS, 657
Wise, J. H., Abel, T., Turk, M. J., Norman, M. L., & Smith, B. D. 2012a, MNRAS, 427, 311
Wise, J. H., Turk, M. J., Norman, M. L., & Abel, T. 2012b, ApJ, 745, 50
Wolcott-Green, J., Haiman, Z., & Bryan, G. L. 2011, MNRAS, 418, 838
Yoshida, N., Abel, T., Hernquist, L., & Sugiyama, N. 2003, ApJ, 592, 645
Yoshida, N., Bromm, V., & Hernquist, L. 2004, ApJ, 605, 579